ACS APPLIED MATERIALS & INTERFACES

Research Article

www.acsami.org

Rapid Atmospheric Pressure Plasma Jet Processed Reduced Graphene Oxide Counter Electrodes for Dye-Sensitized Solar Cells

Hsiao-Wei Liu,[†,⊗] Sheng-ping Liang,[‡,⊗] Ting-Jui Wu,[†,⊗] Haoming Chang,[§] Peng-Kai Kao,[∥] Cheng-Che Hsu,*[,∥] Jian-Zhang Chen,*[,§] Pi-Tai Chou,*[,‡,⊥] and I-Chun Cheng*[,†]

[†]Graduate Institute of Photonics and Optoelectronics, National Taiwan University, No. 1, Sec. 4, Roosevelt Rd., Taipei 10617, Taiwan

[‡]Department of Chemistry, National Taiwan University, No. 1, Sec. 4, Roosevelt Rd., Taipei 10617, Taiwan

[§]Institute of Applied Mechanics, National Taiwan University, No. 1, Sec. 4, Roosevelt Rd., Taipei 10617, Taiwan

[∥]Department of Chemical Engineering, National Taiwan University, No. 1, Sec. 4, Roosevelt Rd., Taipei 10617, Taiwan

[⊥]Center for Emerging Material and Advanced Devices, National Taiwan University, No. 1, Sec. 4, Roosevelt Rd., Taipei 10617, Taiwan

Supporting Information

ABSTRACT: In this work, we present the use of reduced graphene oxide (rGO) as the counter electrode materials in dye-sensitized solar cells (DSSCs). rGO was first deposited on a fluorine-doped tin oxide glass substrate by screen-printing, followed by post-treatment to remove excessive organic additives. We investigated the effect of atmospheric pressure plasma jet (APPJ) treatment on the DSSC performance. A power conversion efficiency of 5.19% was reached when DSSCs with an rGO counter electrode were treated by APPJs in the ambient air for a few seconds. For comparison, it requires a conventional calcination process at 400 °C for 15 min to obtain comparable efficiency. Scanning electron micrographs show that the APPJ treatment modifies the rGO structure, which may reduce its conductivity in part but simultaneously greatly enhances its catalytic activity. Combined with the rapid removal of organic additives by the highly reactive APPJ, DSSCs with APPJ-treated rGO counter electrode show comparable efficiencies to furnace-calcined rGO counter electrodes with greatly reduced process time. This ultrashort process time renders an estimated energy consumption per unit area of 1.1 kJ/cm^2, which is only one-third of that consumed in a conventional furnace calcination process. This new methodology thus saves energy, cost, and time, which is greatly beneficial to future mass production.

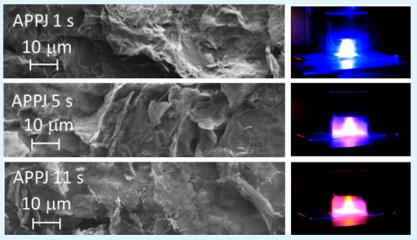

KEYWORDS: *dye-sensitized solar cells, counter electrode, atmospheric pressure plasma jet, graphene oxide, graphene, carbon*

1. INTRODUCTION

Over the past few decades, the impending shortage of fossil-fuel-based energy sources has become a pivotal issue worldwide. Searching for alternative energy sources is currently an intensive research topic. Among all possible options, including wind power and hydroelectric power, solar energy is considered to be a strong candidate for renewable electricity generation because it is widely distributed and essentially unlimited. Unfortunately, despite the tremendous technological advancements achieved in photovoltaic devices, their high cost remains a major obstacle for popularization.

Dye-sensitized solar cells (DSSCs), which are inexpensive and can be fabricated easily, have been studied intensively by researchers worldwide since 1991.[1] A typical DSSC usually comprises a dye-adsorbed nanocrystalline TiO_2 film as an active layer, an electrolyte with a redox couple in either liquid or solid state, and a counter electrode in order to reduce redox species that are used as mediators in the regeneration of the sensitizer after the electron injection.[2−7] As for the liquid electrolytes, in most cases, iodide/tri-iodide (I^-/I_3^-) couple has been used as the redox mediator. Accordingly, platinum is often employed as the counter electrode material owing to its high catalytic ability to I_3^- reduction, high conductivity, and good stability against the corrosion of iodine-based redox electrolytes.[8−10] However, because it is a precious metal, platinum is costly with limiting abundance. This motivates the search for alternative counter electrode materials.[11−17] Carbonaceous materials, which are inexpensive and readily available, are deemed a potential candidate to replace platinum in DSSCs based on their catalytic ability, conductivity, and corrosion stability. Among these carbonaceous materials, graphite,[18] carbon black,[19] activated carbon,[20] and single-walled carbon nanotubes[21] have been used for realizing platinum-free DSSCs.

Ever since its isolation through mechanical exfoliation in 2004,[22] graphene has been attracting considerable attention. Graphene is a one-atom-thick, two-dimensional structure of hexagonally packed carbon atoms that shows remarkable electrical, optical, mechanical, and thermal properties, leading

Received: May 23, 2014
Accepted: August 15, 2014
Published: August 15, 2014

to applications in various fields such as electronics, photovoltaic devices, and energy storage devices. Graphene can be incorporated into the photoanodes of DSSCs to enhance conductivity[23] and light absorption.[24] Meanwhile, they can be used as the counter electrode material to replace platinum.[25−27] In regard to DSSCs with graphene counter electrodes, Zhang et al. have thus far reported the best efficiency of 6.8%.[26] They mixed graphene nanosheets with ethyl cellulose and terpineol to form a graphene paste, which was then coated onto the fluorine-doped tin oxide (FTO) glass via screen-printing process, followed by furnace annealing to remove excess organic binder in the printed graphene film.

Atmospheric pressure plasma technology is advantageous in versatile applications including surface modification, rapid thermal annealing, thin-film deposition, bacteria inactivation, and rapid sintering processes.[5,28−48] Atmospheric pressure plasma jet (APPJ) processes involve the reaction chemistry in the nonthermal plasmas; the participation of oxygen atoms in the plasmas can effectively remove organics by oxidation, rendering rapid processing capability.[28,43,44] In addition, it is a nonvacuum process that is compatible with large-area and roll-to-roll fabrication.[28,44] Atmospheric pressure plasmas (APPs) have been used in many aspects of solar cell fabrication. A 30 min radio frequency (rf) APP has been used for the preparation of TiO_2 photoanodes of on-plastic DSSCs.[28] APPJ-deposited organosilicon was used as the underlayer for the self-texturing of overlaid sputter-deposited Ga-doped ZnO (GZO).[30,46−48] This self-textured GZO was then applied as the front contact for a-Si:H solar cells to enhance the light scattering and light trapping, which thereby improved the cell efficiencies. TiO_2 prepared by modified dielectric barrier discharge (DBD) jet with elevated temperatures was implemented as the photoanodes of DSSCs.[5,33] A DSSC fabricated with the plasma-modified electrospun poly(vinylidenefluoride-*co*-hexafluoropropylene) membrane electrolyte revealed improved conversion efficiency.[40] Improved performance of DSSCs with TiO_2 treated by atmospheric-pressure nonequilibrium direct current (DC) pulse discharge plasma jet[49,50] and DBD-treatment[51] have been demonstrated. Atmospheric pressure plasma TiO_2 coating was also suggested for the protection layer of plastic substrates for DSSCs.[52,53] In addition to the application of nonthermal-equilibrium plasmas to solar cell fabrication, some thermal-plasma techniques have been used for the annealing of ZnO:Al films and recrystallization of amorphous Si for Si thin-film solar cells.[32,34,35]

In our previous studies, we have demonstrated DSSCs with TiO_2 photoanodes rapidly sintered by APPJs; the sintering time (∼1 min) was greatly reduced compared to that for conventional furnace calcination (>15 min).[43] The temperature of rapid APPJ-sintering process can be further lowered from ∼500 °C to ∼300 °C by introducing O_2 in the APPJs.[44] In this study, we then made a new attempt by treating the graphene counter electrodes, which was made by screen printing process, with APPJ instead of with conventional furnace calcination process. To our surprise, DSSCs with APPJ-treated reduced graphene oxide (rGO) counter electrodes showed efficiencies comparable to those of furnace-calcined counter electrode while requiring a much shorter process time. APPJ treatment for 11 s is sufficient to fabricate well-functioning rGO counter electrodes for DSSCs. This, together with rGO based electrodes, effectively reduces the time and cost of DSSC production.

2. EXPERIMENTAL DETAILS

To fabricate the photoanode, a 0.075 M titanium isopropoxide solution (Acros Organics) was first spin-coated onto FTO glass (TEC7; thickness, 2.2 mm; transmittance, >80%; sheet resistance, 8 Ω·cm; Pilkington Group, Ltd.) and then baked in air at 200 °C for 10 min to form a compact TiO_2 layer. Next, a commercial TiO_2 paste with TiO_2 particle size of 20−50 nm (E-solar P300, Everlight Chemical Industrial Co.) was screen-printed on the substrate three times to form the nanocrystalline layer, following which a scattering layer was printed using another commercial TiO_2 paste with TiO_2 particle size of 250−300 nm (E-solar P400, Everlight Chemical Industrial Co.). Between each screen-printing step, the sample was heated at 100 °C for 10 min to dry off the solvents. The ∼11 μm thick TiO_2 layer was finally sintered at 510 °C in air for 15 min using a tube furnace, followed by immersion in a 0.05 M $TiCl_4$ solution (Showa Chemical Co.) at 70 °C for 30 min. After rinsing with ethanol, the TiO_2 photoanode was furnace-calcined again at 510 °C for 15 min.

A graphene counter electrode was also fabricated by screen-printing with pastes containing rGO (TNRGO, TimesGraph). To prepare this paste, we first mixed ethyl cellulose (30−70 mPa s, SIGMA) with alpha-terpineol (97+%, ACROS) in a ratio of 1:10 by weight to form a viscous solution. Next, the rGO was dispersed in ethanol and then mixed with the ethyl cellulose/alpha-terpineol solution. Finally, the rGO paste was obtained by evaporating ethanol from alpha-terpineol in the mixed solution using a rotary evaporator. The screen-printed rGO film was then treated by N_2 APPJ for 1, 5, 9, 11, 13, 17, and 120 s. The APPJ system is described in detail in references.[39,43,44,54] The APPJ system was operated with a 30 slm N_2 flow, 275 V applied voltage, and 7/33 μs on/off duty cycle. The sample was located on an $x-y$ moving stage located at the downstream of the plasma jet, and the film was treated for the designated durations under the exposure to the plasma jet; the stage was retreated after the treatment. In order to confine the plasma jet and minimize the influence of the ambient air on the jet behavior, the jet exit is surrounded by a glass tube 3 cm in diameter. The distance between the stage and the plasma jet nozzle was 2 cm, and the gap between the glass tube exit and the stage was kept at 1 mm. The substrate temperature reaches ∼400 °C owing to plasma heating during treatment. For comparison, reference Pt and rGO counter electrodes were prepared by spin-coating of chloroplatinic acid hydrate (99.95%, H_2PtCl_6, Uniregion biotech) solution and screen-printing with pastes containing rGO onto FTO glass substrates, respectively. The counterparts were then calcined at 400 °C in air for 15 min using a tube furnace, which has a 15 cm flat-temperature zone and is equipped with a quartz tube 8 cm in diameter. The power consumption of this furnace is 4 kW.

To complete DSSC fabrication, we immersed sintered TiO_2 nanoporous films in a mixed solution of acetonitrile (99.9%, J. T. Baker) and tertiary butyl alcohol (99.9%, J. T. Baker) containing 3×10^{-4} M of N719 dye (Solaronix) for 23 h. After the anchoring of dyes, the photoanodes were rinsed with ethanol and dried at room temperature. The dye-adsorbed photoanodes were then assembled with calcined graphene counter electrodes with a 25 μm spacer in between. Finally, a liquid electrolyte (Eversolar EL 100, Everlight Chemical Industrial Co.) consisting of I_2, LiI, guanidinium thiocyanate (GuNCS), and acetonitrile was injected into the assembled cells.

To evaluate the DSSC performance, we placed the cells on a dark background and illuminated them through the FTO glass substrates using a solar simulator (WACOM, WXS-155S-L2) with an AM1.5 filter. During the measurement, the incident light was confined within a small area of 0.16 cm^2 by a stainless steel mask. A Keithley 2400 electrometer was used to measure the $I-V$ characteristics. The incident-photon-to-current-conversion efficiency (IPCE) was acquired by a solar cell quantum efficiency measurement system (PV Measurements, QEX10). The monochromatic light was modulated at a frequency of 100 Hz, and the resulting modulated current was analyzed by using a lock-in amplifier. Electrochemical impedance spectroscopy (EIS) analysis was performed on the complete cells using an electrochemical workstation (Zahner Zennium). The EIS spectra were obtained by applying sinusoidal perturbations of ±10 mV with

frequencies ranging from 0.1 to 10^5 Hz and at DC bias voltages equal to the open circuit voltages of the cells under illumination.

The surface morphology of the rGO counter electrodes was investigated by scanning electron microscopy (SEM, Nova NanoSEM 230, FEI). The chemical composition was analyzed by X-ray photoelectron spectroscopy (XPS, ThermoScientific, Theta Probe) using a monochromated Al Kα X-ray source.

3. RESULTS AND DISCUSSION

Figure 1a shows the $I-V$ characteristics of DSSCs with the Pt counter electrode and rGO counter electrodes treated by

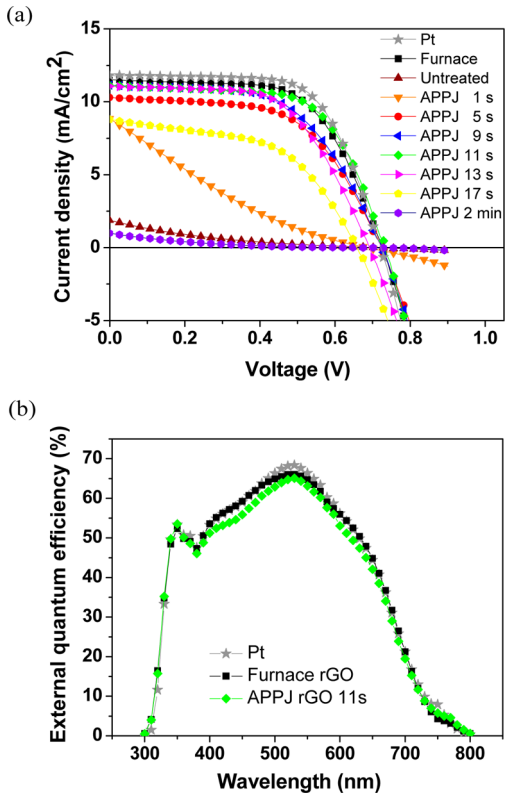

Figure 1. (a) $I-V$ curves of DSSCs with Pt and rGO counter electrodes treated by various methods. (b) Incident photon-to-current conversion efficiencies of DSSCs with Pt, furnace-calcined rGO, and rGO counter electrodes treated with APPJ for 11 s.

various methods, and the corresponding photovoltaic parameters are listed in Table 1. The photoelectric conversion efficiency of the DSSC using untreated rGO counter electrode is extremely low (0.19%) owing to the incomplete removal of organic binders in the rGO paste, the result of which implies the necessity of post-treatment. As for DSSCs with APPJ-treated rGO counter electrodes, the cell performance improves and then degrades with increasing treatment duration. DSSCs with rGO counter electrode treated by APPJ for 11 s show a maximum efficiency of 5.19% under illumination of 100 mW cm^{-2}, which is slightly less than that of the reference cell with a Pt counter electrode but comparable to that of the reference cell using a furnace-calcined rGO counter electrode. The incident photon-to-current conversion efficiencies of the cell with rGO counter electrode treated by APPJ for 11 s and the reference cells are plotted in Figure 1b. Similar results are observed. Clearly, by using APPJs, the time for processing the rGO counter electrode can be significantly reduced without sacrificing cell performance.

Table 1. Photovoltaic Parameters of DSSCs with Pt and rGO Counter Electrodes Treated by Various Methods

counter electrode	open-circuit voltage, V_{OC} (V)	short-circuit current density, J_{SC} (mA/cm^2)	fill factor, FF(%)	efficiency, η (%)
Pt	0.73	11.80	65.75	5.65
furnace rGO	0.73	11.50	62.25	5.19
untreated rGO	0.71	1.88	14.29	0.19
APPJ rGO 1 s	0.68	8.81	19.03	1.14
APPJ rGO 5 s	0.72	10.29	57.36	4.28
APPJ rGO 9 s	0.72	11.13	57.09	4.60
APPJ rGO 11 s	0.73	11.11	63.82	5.19
APPJ rGO 13 s	0.69	11.07	58.48	4.48
APPJ rGO 17 s	0.66	8.76	39.95	3.01
APPJ rGO 2 min	0.67	0.99	12.15	0.08

Figure 2 shows the Nyquist plots of the EIS results of the DSSCs with rGO counter electrodes under illumination of 100

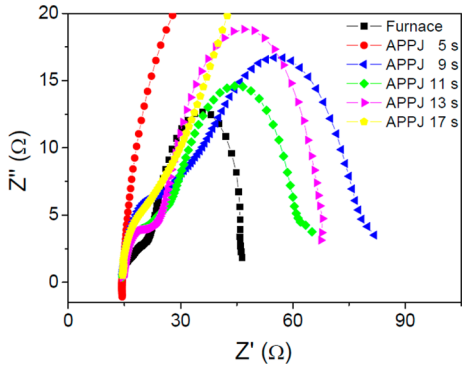

Figure 2. Nyquist plots of EIS results of DSSCs with rGO counter electrodes treated by APPJ for various durations and by furnace calcination.

mW cm^{-2}. The first semicircle corresponds to the redox reaction at the counter electrode. A detailed equivalent circuit model can be found in literature.[55] As a result, the charge transfer resistance at the interface between the counter electrode and the electrolyte redox reaction (R_{CE}) as a function of APPJ treatment duration is shown in Figure 3. R_{CE} decreases significantly as the APPJ treatment duration increases from 1 to 9 s, owing to the rapid removal of excessive organic binder by APPJs. At a treatment duration of 9–13 s, the values of R_{CE} are comparable to those of furnace-calcined counter electrodes (14.26 Ω). A further increase in the APPJ treatment duration may cause the removal of rGO and thus a decrease in catalytic ability. The negative correlation between R_{CE} and solar cell efficiency suggests that the enhancement in photovoltaic performance is derived from the improved catalytic ability of the rGO counter electrodes to I_3^-/I^- reduction.

Figures 4 and 5 show scanning electron micrographs of rGO counter electrodes treated by various methods. An as-screen-printed rGO counter electrode has a rough surface lacking an obvious sheet structure. Furnace calcination removes the

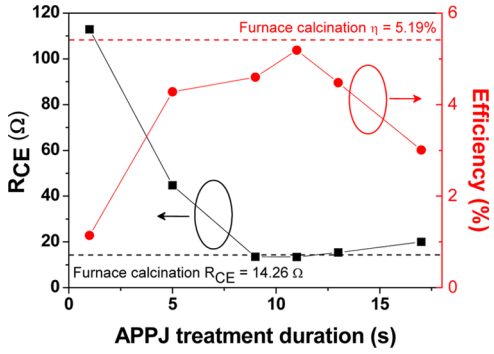

Figure 3. R_{CE} and cell efficiency as functions of APPJ treatment duration.

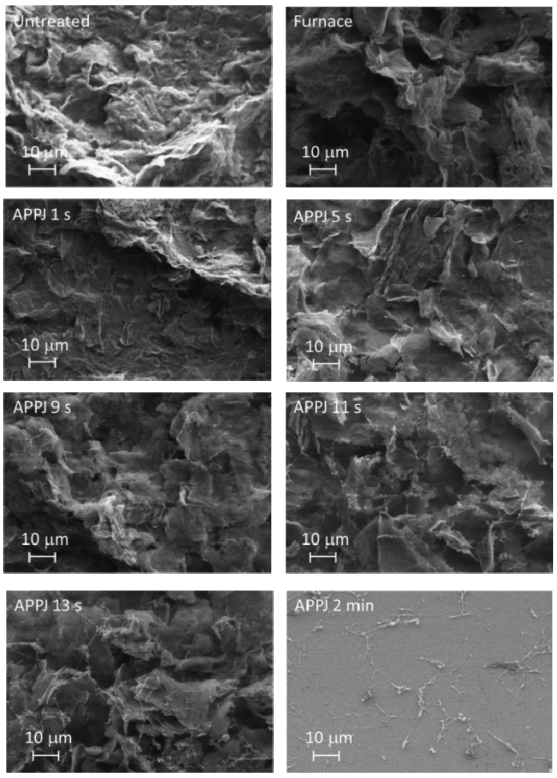

Figure 4. Scanning electron micrographs of rGO counter electrodes treated by various methods (1000×).

organic binder from the screen-printed counter electrode, and the sheet structure of the rGO along with cracks and gaps is revealed. For APPJ-treated counter electrodes, the cracks and protruding flakes become more evident as the treatment duration increases. When the treatment duration is extended to 2 min, only a small fraction of rGO remains on the FTO glass substrate; most rGO has been removed by the plasma. N_2 plasmas are known for their high reactivity because of the existing excited nitrogen molecules. The transitions of excited nitrogen molecules, N_2 first positive $B^3\Pi_g \rightarrow A^3\sum_u^+$ and second positive $C^3\Pi_u \rightarrow B^3\Pi_g$, release over 6 eV of energy.[56] These highly energetic N_2 molecules in APPJs provide sufficient energy to assist the fast removal of organic binders but also cause defect creation and eventual removal of rGO. As shown in Figure 5, while the counter electrodes calcined in a furnace or treated with APPJ for 1 s show an intact rGO sheet structure, gaps and defects emerge for the APPJ-treated counter electrodes with a duration exceeding 5 s. Defects and oxidic

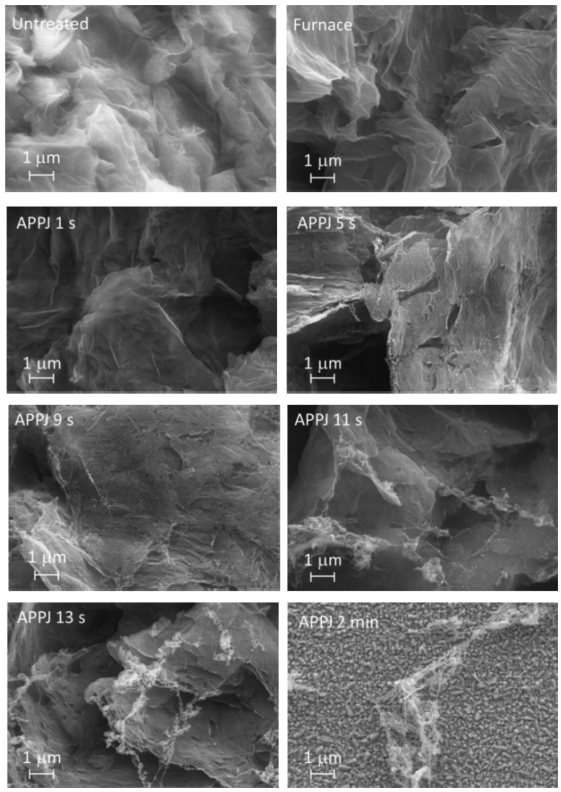

Figure 5. Scanning electron micrographs of rGO counter electrodes treated by various methods (10 000×).

surface groups are the active sites for catalyzing I_3^-/I^- reduction,[57,58] and higher defect density may result in stronger catalytic ability, as indicated by the R_{CE} values shown in Figure 3. APPJ treatments may remove organic binder rapidly and damage the rGO structure at the same time, suppressing conductivity of the counter electrode in DSSC. The negative impact of the inferior conductivity might be counteracted by the superior catalytic activity of APPJ-treated rGO, showing a comparable performance to 15 min furnace calcination at a treatment duration of 11 s.

We then examine the chemical composition of the APPJ-treated counter electrodes by XPS. Figure 6 shows the C(1s) spectra of the counter electrodes treated by the APPJ for 1, 5, 11, and 17 s. It is worth noting that throughout the samples tested, no observable signal was obtained in the N(1s) scan. This suggests that nearly no nitrogen doping occurs in the APPJ-treated samples, most likely due to the short treatment duration. For C(1s) scans with 1 and 5 s treatment duration, we observe three peaks at 284.5, 286.3, and 288.5 eV, which can be assigned to C−C, C−O, and C═O, respectively. The strong C−O peak is due to the existence of additives in the paste, namely ethyl cellulose, in addition to rGO. With an increase in the APPJ treatment duration, the reduction of the C−O and C═O peaks clearly indicates the effective removal of the additives by the interaction between the APPJ and the paste. For samples with a treatment duration of 11 s and above, the major composition of C(1s) scan is C−C, with a small amount of C−O and C═O. This clearly shows the removal of the additives and the retaining of rGO, as reported in literature.[59,60]

To further elucidate the interaction between the APPJ and the treated counter electrodes, we then examine time-resolved photo images and optical emission spectra emanating from the

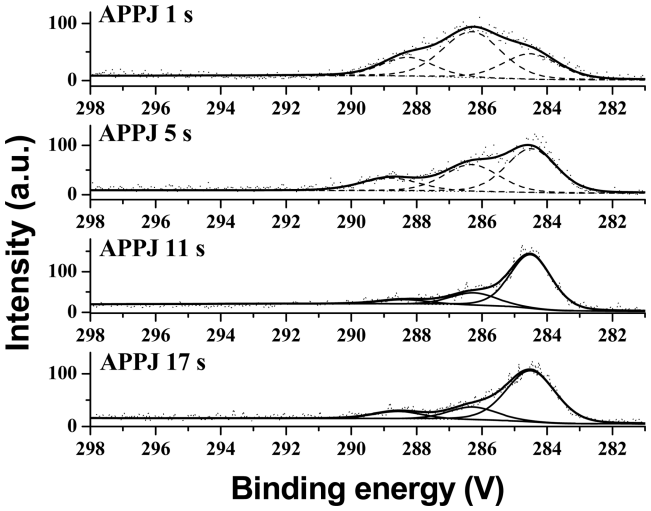

Figure 6. XPS C(1s) spectra of rGO counter electrodes treated by APPJ for different durations.

plasma. When the counter electrode is treated by the APPJ, the color of the APPJ inspected visually changes drastically with time, as shown in Figure 7. The color is initially bluish and

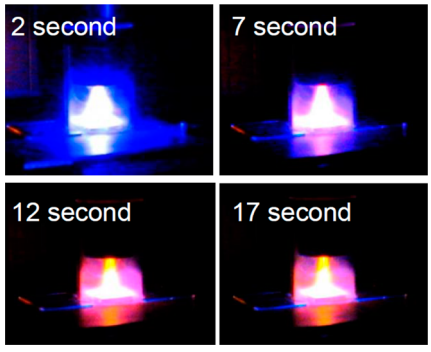

Figure 7. Visual appearance of the plasma jet at selected times examined by a digital camera.

turns yellow and orange as the treatment duration increases. Such an observation strongly suggests the change in the plasma species throughout the APPJ-treatment process due to the reaction between the APPJ and the paste.

The optical emission spectra emanating from the APPJ during the treatment process are shown in Figure 8. The spectrum acquired without the existence of the treated electrode is also shown for comparison. The assignment of each major emission bands are also labeled in Figure 8. It clearly shows the existence of the CN violet system ($B^2\sum \rightarrow X^2\sum$). The blue color shown in the photo images in Figure 7 (2 s) is originated from the strong emission of this emission system at the wavelengths below 450 nm. At the early stage of APPJ treatment, very strong CN emission is observed, which indicates the reaction between the plasma and the carbon content, binder and/or rGO, in the paste. With an increase in the treatment duration, the CN emission decreases rapidly. At 12 s, very weak CN emission is observed. At this stage, the emission is dominant by N_2 second positive system, which shows a yellow/orange color, as reported previously.[61] To identify the key component in the paste that reacts with the APPJ then emanates the CN violet system, we prepared a test paste with the same procedure and composition but without

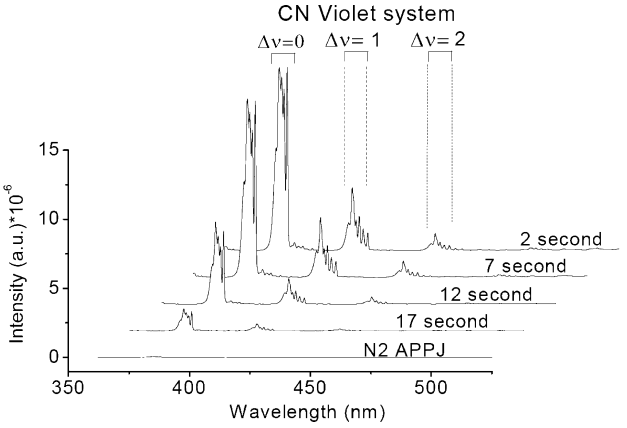

Figure 8. Time resolved optical emission spectra emanating from the APPJ acquired at different times and the spectrum obtained without the existence of the paste-coated electrode.

the addition of rGO. When this test paste was treated by the APPJ, a nearly identical emission was observed. Such an observation shows that the CN emission is primarily associated with the reaction of the APPJ with ethyl cellulose, rather than with rGO. The selective removal of ethyl cellulose while retaining rGO renders such an APPJ-based process a rapid process for DSSC counter electrode fabrication.

We further examine the time-resolved intensity of the emission at 388.3 nm ($\nu' = 0 \rightarrow \nu'' = 0$, $B^2\sum \rightarrow X^2\sum$) in the process, and the result is shown in Figure 9. A rapid rising

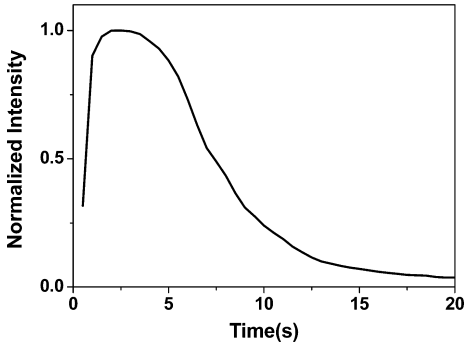

Figure 9. Normalized time-resolved intensity of the optical emission at 388.3 nm ($\nu' = 0 \rightarrow \nu'' = 0$, $B^2\sum \rightarrow X^2\sum$) during the APPJ treatment process.

followed by a gradual decrease in the emission intensity is observed. The emission intensity drops to below 20% of the maximum value at time between 10 and 12 s. Such an observation is consistent with the optimal APPJ treatment duration of ~11 s based on the cell performance shown above. It also indicates that the APPJ emission is capable of serving as the process end point detection, and it has been widely used in plasma etching processes.

To perform economical assessment in terms of energy efficiency of this present APPJ-based process and the conventional furnace calcination process, we compare the energy consumptions of these two processes. In a thermal calcination process with a tube furnace presently used, substrates with a total area of 120 cm^2 can be treated simultaneously, and a 15 min treatment consumes energy of 360 kJ by assuming 10% of the total power output is required to maintain a temperature of 400 °C. This yields an energy

consumption per unit area of 3 kJ/cm^2. Such estimation gives a lower bound of the energy consumption of the furnace calcination process. In the APPJ process, the treated area is 7 cm^2, which is the cross-sectional area of the glass tube located at the jet downstream. Under the operating condition described in the Experimental Details, the power output of the power source is approximately 700 W. An 11 s treatment, together with the effective treated area, yields an energy consumption per unit area of 1.1 kJ/cm^2. Moreover, we note that the effective treated area of this APPJ can be further increased by a factor of 4 rather easily when a glass tube with a larger diameter is used in the jet downstream, as reported previously.[62] This comparison shows that the APPJ-based process can potentially serve as an energy-saving process.

In addition to the low energy consumption described above, the rapid APPJ-based treatment offers great process significance in the follow aspects. First, such a technique is much more readily implemented into large-area processes. For example, an APPJ-based process can be much more easily integrated to a roll-to-roll process, an emerging industrial process, compared with a calcination process utilizing a furnace. Second, when a high throughput is desired, an APPJ-based system equipped with multiple jets in parallel can be easily adopted as a straightforward and effective approach. Finally, due to the short treatment duration and the compact size of the APPJ, the system requires a small footprint. These advantages render the APPJ-based process a promising alternative to the conventional furnace calcination processes in a great number of applications.

4. CONCLUSION

In summary, a counter electrode utilizing rGO for DSSCs was reported. Different from other methods, the electrode was prepared by mixing rGO with alpha-terpineol and ethyl cellulose to form a viscous paste and coated on an FTO glass substrate through screen-printing. Subsequent calcination was treated by APPJ rather than the conventional furnace process. The effect of APPJ treatment on the screen-printed rGO film was then carefully investigated. The DSSC with rGO counter electrode treated by APPJ for 11 s shows an efficiency of 5.19% that is comparable to that of the DSSC using a 15 min furnace-calcined rGO counter electrode, demonstrating the validity of APPJ as a rapid-treatment technique to produce graphene-based counter electrodes for DSSCs. Insight into the associated mechanism is provided by EIS and scanning electron micrographs, unveiling the catalytic ability and morphology of the rGO counter electrode, respectively, as a function of the APPJ treatment duration. A treatment duration of 9−13 s reveals R_{CE} and morphology of the rGO counter electrode comparable to that of the furnace-calcined counterpart. The major scope is to demonstrate an ultrarapid and cost-effective APPJ treatment to fabricate rGO counter electrodes that is able to effectively remove the binders while retaining the major microstructure, chemical composition, and electrocatalytic activity of rGO. The SEM, XPS analyses and cell performance tests strongly suggest the retaining of the rGO key features described above. APPJ can thus be used in the DSSC fabrication process to reduce the processing time and thermal budget, hence reducing the fabrication cost and energy payback time. Rapid APPJ treatments can also be applied to the roll-to-roll process to increase the substrate conveying speed, paving a facile avenue en route to economic DSSC production.

■ ASSOCIATED CONTENT

Supporting Information

Comparison of photovoltaic parameters of DSSCs with Pt and rGO counter electrodes. This material is available free of charge via the Internet at http://pubs.acs.org.

■ AUTHOR INFORMATION

Corresponding Authors

*I-C.C. Tel.: 886 2-33669648. E-mail: iccheng@ntu.edu.tw.
*P.-T.C. Tel.: 886 2-33663894. E-mail: chop@ntu.edu.tw.
*J.-Z.C. Tel.: +886 2-33665694. E-mail: jchen@ntu.edu.tw.
*C.-C.H. Tel.: +886 2-33663034. E-mail: chsu@ntu.edu.tw.

Author Contributions

⊗These authors contributed equally to this work.

Notes

The authors declare no competing financial interest.

■ ACKNOWLEDGMENTS

This research was funded by the Center for Emerging Material and Advanced Devices, National Taiwan University. The authors also gratefully acknowledge funding support from the Ministry of Science and Technology, Taiwan, under Grants MOST 101-2628-E-002-020-MY3, MOST 102-2221-E-002-060, and MOST 102-3113-P-002-027.

■ REFERENCES

(1) O'Regan, B.; Grätzel, M. A Low-Cost, High-Efficiency Solar Cell Based on Dye-Sensitized Colloidal TiO_2 Films. *Nature* **1991**, *35*, 737−739.

(2) Grätzel, M. The Advent of Mesoscopic Injection Solar Cells. *Prog. Photovoltaics* **2006**, *14*, 429−442.

(3) Yen, M. Y.; Hsiao, M. C.; Liao, S. H.; Liu, P. I.; Tsai, H. M.; Ma, C. C. M.; Pu, N. W.; Ger, M. D. Preparation of Graphene/Multi-Walled Carbon Nanotube Hybrid and Its Use As Photoanodes of Dye-Sensitized Solar Cells. *Carbon* **2011**, *49*, 3597−3606.

(4) Park, S. H.; Lim, J.; Kwon, Y. S.; Song, I. Y.; Choi, J. M.; Song, S.; Park, T. Tunable Nanoporous Network Polymer Nanocomposites Having Size-Selective Ion Transfer for Dye-Sensitized Solar Cells. *Adv. Energy Mater.* **2013**, *3*, 184−192.

(5) Seo, H. K.; Elliott, C. M.; Shin, H. S. Mesoporous TiO_2 Films Fabricated Using Atmospheric Pressure Dielectric Barrier Discharge Jet. *ACS Appl. Mater. Interfaces* **2010**, *2*, 3397−3400.

(6) Chen, C. Y.; Wang, M. K.; Li, J. Y.; Pootrakulchote, N.; Alibabaei, L.; Ngoc-le, C. H.; Decoppet, J. D.; Tsai, J. H.; Grätzel, C.; Wu, C. G.; Zakeeruddin, S. M.; Grätzel, M. Highly Efficient Light-Harvesting Ruthenium Sensitizer for Thin-Film Dye-Sensitized Solar Cells. *ACS Nano* **2009**, *3*, 3103−3109.

(7) Yella, A.; Lee, H. W.; Tsao, H. N.; Yi, C. Y.; Chandiran, A. K.; Nazeeruddin, M. K.; Diau, E. W. G.; Yeh, C. Y.; Zakeeruddin, S. M.; Grätzel, M. Porphyrin-Sensitized Solar Cells with Cobalt (II/III)-Based Redox Electrolyte Exceed 12% Efficiency. *Science* **2011**, *334*, 629−634.

(8) Luo, Y. H.; Li, D. M.; Meng, Q. B. Towards Optimization of Materials for Dye-Sensitized Solar Cells. *Adv. Mater.* **2009**, *21*, 4647−4651.

(9) Papageorgiou, N.; Maier, W. F.; Grätzel, M. An Iodine/Triiodide Reduction Electrocatalyst for Aqueous and Organic Media. *J. Electrochem. Soc.* **1997**, *144*, 876−884.

(10) Kim, S. S.; Nah, Y. C.; Noh, Y. Y.; Jo, J.; Kim, D. Y. Electrodeposited Pt for Cost-Efficient and Flexible Dye-Sensitized Solar Cells. *Electrochim. Acta* **2006**, *51*, 3814−3819.

(11) Murakami, T. N.; Grätzel, M. Counter Electrodes for DSC: Application of Functional Materials as Catalysts. *Inorg. Chim. Acta* **2008**, *361*, 572−580.

(12) Trevisan, R.; Dobbelin, M.; Boix, P. P.; Barea, E. M.; Tena-Zaera, R.; Mora-Sero, I.; Bisquert, J. PEDOT Nanotube Arrays as High Performing Counter Electrodes for Dye Sensitized Solar Cells. Study of the Interactions Among Electrolytes and Counter Electrodes. *Adv. Energy Mater.* **2011**, *1*, 781−784.
(13) Guai, G. H.; Leiw, M. Y.; Ng, C. M.; Li, C. M. Sulfur-Doped Nickel Oxide Thin Film as an Alternative to Pt for Dye-Sensitized Solar Cell Counter Electrodes. *Adv. Energy Mater.* **2012**, *2*, 334−338.
(14) Bi, H.; Zhao, W.; Sun, S. R.; Cui, H. L.; Lin, T. Q.; Huang, F. Q.; Xie, X. M.; Jiang, M. H. Graphene Films Decorated with Metal Sulfide Nanoparticles for Use as Counter Electrodes of Dye-Sensitized Solar Cells. *Carbon* **2013**, *61*, 116−123.
(15) Wang, R.; Wu, Q. D.; Lu, Y.; Liu, H. W.; Xia, Y. Z.; Liu, J. Q.; Yang, D. J.; Huo, Z. Y.; Yao, X. D. Preparation of Nitrogen-Doped TiO_2/Graphene Nanohybrids and Application as Counter Electrode for Dye-Sensitized Solar Cells. *ACS Appl. Mater. Interfaces* **2014**, *6*, 2118−2124.
(16) Peng, T.; Sun, W. W.; Huang, C. L.; Yu, W. J.; Sebo, B.; Dai, Z. G.; Guo, S. S.; Zhao, X. Z. Self-Assembled Free-Standing Polypyrrole Nanotube Membrane as an Efficient FTO- and Pt-Free Counter Electrode for Dye-Sensitized Solar Cells. *ACS Appl. Mater. Interfaces* **2014**, *6*, 14−17.
(17) Zeng, W.; Fang, G. J.; Li, B. R.; Liu, Z. Q.; Han, T. Y.; Wang, J.; Liu, F. W.; Fang, P. F.; Zhao, X. Z.; Zou, D. C. Vibration Test Method to Study Elastic Stability of Porous Carbon Nanocomposite Counter Electrode in Dye Sensitized Solar Cells. *ACS Appl. Mater. Interfaces* **2013**, *5*, 7101−7108.
(18) Kay, A.; Grätzel, M. Low Cost Photovoltaic Modules based on Dye Sensitized Nanocrystalline Titanium Dioxide and Carbon Powder. *Sol. Energy Mater. Sol. Cells* **1996**, *44*, 99−117.
(19) Murakami, T. N.; Ito, S.; Wang, Q.; Nazeeruddin, M. K.; Bessho, T.; Cesar, I.; Liska, P.; Humphry-Baker, R.; Comte, P.; Pechy, P.; Grätzel, M. Highly Efficient Dye-Sensitized Solar Cells Based on Carbon Black Counter Electrodes. *J. Electrochem. Soc.* **2006**, *153*, A2255−A2261.
(20) Imoto, K.; Takahashi, K.; Yamaguchi, T.; Komura, T.; Nakamura, J.; Murata, K. High-Performance Carbon Counter Electrode for Dye-Sensitized Solar Cells. *Sol. Energy Mater. Sol. Cells* **2003**, *79*, 459−469.
(21) Suzuki, K.; Yamaguchi, M.; Kumagai, M.; Yanagida, S. Application of Carbon Nanotubes to Counter Electrodes of Dye-Sensitized Solar Cells. *Chem. Lett.* **2003**, *32*, 28−29.
(22) Novoselov, K. S.; Geim, A. K.; Morozov, S. V.; Jiang, D.; Zhang, Y.; Dubonos, S. V.; Grigorieva, I. V.; Firsov, A. A. Electric Field Effect in Atomically Thin Carbon Films. *Science* **2004**, *306*, 666−669.
(23) Yang, N. L.; Zhai, J.; Wang, D.; Chen, Y. S.; Jiang, L. Two-Dimensional Graphene Bridges Enhanced Photoinduced Charge Transport in Dye-Sensitized Solar Cells. *ACS Nano* **2010**, *4*, 887−894.
(24) Yan, X.; Cui, X.; Li, B. S.; Li, L. S. Large, Solution-Processable Graphene Quantum Dots as Light Absorbers for Photovoltaics. *Nano Lett.* **2010**, *10*, 1869−1873.
(25) Kaniyoor, A.; Ramaprabhu, S. Thermally Exfoliated Graphene Based Counter Electrode for Low Cost Dye Sensitized Solar Cells. *J. Appl. Phys.* **2011**, *109*, 124308.
(26) Zhang, D. W.; Li, X. D.; Li, H. B.; Chen, S.; Sun, Z.; Yin, X. J.; Huang, S. M. Graphene-Based Counter Electrode for Dye-Sensitized Solar Cells. *Carbon* **2011**, *49*, 5382−5388.
(27) Wang, H.; Hu, Y. H. Graphene as a Counter Electrode Material for Dye-Sensitized Solar Cells. *Energy Environ. Sci.* **2012**, *5*, 8182−8188.
(28) Jung, H.; Park, J.; Yoo, E. S.; Han, G. S.; Jung, H. S.; Ko, M. J.; Park, S.; Choe, W. Functionalization of Nanomaterials by Non-Thermal Large Area Atmospheric Pressure Plasmas: Application to Flexible Dye-Sensitized Solar Cells. *Nanoscale* **2013**, *5*, 7825−7830.
(29) Zheng, X.; Chen, G. L.; Zhang, Z. X.; Beem, J.; Massey, S.; Huang, J. F. A Two-Step Process for Surface Modification of Poly(ethylene terephthalate) Fabrics by Ar/O_2 Plasma-Induced Facile Polymerization at Ambient Conditions. *Surf. Coat. Technol.* **2013**, *226*, 123−129.
(30) Yu, S. H.; Ho, P. C.; Yang, T. W.; Bi, C. C.; Yeh, C. H.; Chang, C. Y. Double-Pattern Textured ZnO:Ga Thin Films Fabricated by an APPJ and an DC Sputtering. *ECS Solid State Lett.* **2012**, *1*, 48−50.
(31) van Gils, C. A. J.; Hofmann, S.; Boekema, B. K. H. L.; Brandenburg, R.; Bruggeman, P. J. Mechanisms of Bacterial Inactivation in the Liquid Phase Induced by a Remote RF Cold Atmospheric Pressure Plasma Jet. *J. Phys. D: Appl. Phys.* **2013**, *46*, 175203.
(32) Shirai, H.; Sakurai, Y.; Yeo, M.; Kobayashi, T.; Ishikawa, T. Rapid Crystallization of Amorphous Silicon Utilizing a VHF Plasma Annealing at Atmospheric Pressure. *Eur. Phys. J.: Appl. Phys.* **2007**, *37*, 315−322.
(33) Seo, H. K.; Fisher, E. R.; Elliott, C. M.; Shin, H. S. Fast One-Step Method to Synthesize TiO_2 Nanoparticle Clusters for Dye Sensitized Solar Cells. *J. Nanosci. Nanotechnol.* **2012**, *12*, 6276−6282.
(34) Ryo, M.; Sakurai, Y.; Kobayashi, T.; Shirai, H. Rapid Recrystallization of Amorphous Silicon Utilizing Very-High-Frequency Microplasma Jet at Atmospheric Pressure. *Jpn. J. Appl. Phys., Part 1* **2006**, *45*, 8484−8487.
(35) Ohta, N.; Ohba, D.; Sato, S.; Tang, Z.; Shimizu, H.; Shirai, H. Rapid Thermal-Plasma Annealing of ZnO:Al Films for Silicon Thin-Film Solar Cells. *Thin Solid Films* **2011**, *519*, 6920−6927.
(36) Liu, L. Y.; Zhang, J. L.; Guo, Q. C.; Wang, D. Z. Diagnostics of the Atmospheric Pressure Plasma Jets for Plasma Enhanced Chemical Vapor Deposition of Polycrystalline Silicon Thin Film. *Acta Phys. Sin.* **2010**, *59*, 2653−2660.
(37) Lien, S. T.; Li, H. C.; Yang, Y. J.; Hsu, C. C.; Cheng, I. C.; Chen, J. Z. Atmospheric Pressure Plasma Jet Annealed ZnO Films for MgZnO/ZnO Heterojunctions. *J. Phys. D: Appl. Phys.* **2013**, *46*, 075202.
(38) Lien, S. T.; Chen, J. Z.; Yang, Y. J.; Hsu, C. C.; Cheng, I. C. Sol-Gel Derived Amorphous/Nanocrystalline MgZnO Thin Films Annealed by Atmospheric Pressure Plasma Jets. *Ceram. Int.* **2014**, *40*, 2707−2715.
(39) Liao, W. Y.; Chang, H. M.; Yang, Y. J.; Hsu, C. C.; Cheng, I. C.; Chen, J. Z. Oxygen-Deficient Indium Tin Oxide Thin Films Annealed by Atmospheric Pressure Plasma Jets with/without Air-Quenching. *Appl. Surf. Sci.* **2014**, *292*, 213−218.
(40) Huang, C.; Lin, P. J.; Tsai, C. Y.; Juang, R. S. Electrospun Microfibrous Membranes with Atmospheric-Pressure Plasma Surface Modification for the Application in Dye-Sensitized Solar Cells. *Plasma Processes Polym.* **2013**, *10*, 938−947.
(41) Homola, T.; Matousek, J.; Medvecka, V.; Zahoranova, A.; Kormunda, M.; Kovacik, D.; Cernak, M. Atmospheric Pressure Diffuse Plasma in Ambient Air for ITO Surface Cleaning. *Appl. Surf. Sci.* **2012**, *258*, 7135−7139.
(42) Foest, R.; Kindel, E.; Ohl, A.; Stieber, M.; Weltmann, K. D. Non-Thermal Atmospheric Pressure Discharges for Surface Modification. *Plasma Phys. Controlled Fusion* **2005**, *47*, B525−B536.
(43) Chang, H.; Yang, Y. J.; Li, H. C.; Hsu, C. C.; Cheng, I. C.; Chen, J. Z. Preparation of Nanoporous TiO_2 Films for DSSC Application by a Rapid Atmospheric Pressure Plasma Jet Sintering Process. *J. Power Sources* **2013**, *234*, 16−22.
(44) Chang, H.; Hsu, C. M.; Kao, P. K.; Yang, Y. J.; Hsu, C. C.; Cheng, I. C.; Chen, J. Z. Dye-Sensitized Solar Cells with Nanoporous TiO_2 Photoanodes Sintered by N_2 and air Atmospheric Pressure Plasma Jets with/without Air-Quenching. *J. Power Sources* **2014**, *251*, 215−221.
(45) Bartis, E. A. J.; Graves, D. B.; Seog, J.; Oehrlein, G. S. Atmospheric Pressure Plasma Treatment of Lipopolysaccharide in a Controlled Environment. *J. Phys. D: Appl. Phys.* **2013**, *46*, 312002.
(46) Yu, S. H.; Ho, P. C.; Lee, C. L.; Bi, C. C.; Yeh, C. H.; Chang, C. Y. Cost-Effective and Self-Textured Gallium-Doped Zinc Oxide Front Contacts for Hydrogenated Amorphous Silicon Thin-Film Solar Cells. *Appl. Phys. Express* **2013**, *6*, 022301.
(47) Chang, K. M.; Ho, P. C.; Yu, S. H.; Hsu, J. M.; Yang, K. H.; Wu, C. J.; Chang, C. C. Using SiO_x Nano-Films to Enhance GZO Thin Films Properties as Front Electrodes of a-Si Solar Cells. *Appl. Surf. Sci.* **2013**, *276*, 756−760.

(48) Chang, K. M.; Ho, P. C.; Ariyarit, A.; Yang, K. H.; Hsu, J. M.; Wu, C. J.; Chang, C. C. Enhancement of the Light-Scattering Ability of Ga-doped ZnO Thin Films Using SiO_x Nano-Films Prepared by Atmospheric Pressure Plasma Deposition System. *Thin Solid Films* **2013**, *548*, 460−464.
(49) Yuji, T.; Sung, Y. M. Surface Treatment of TiO_2 Films by Pulse Plasma for Dye-Sensitized Solar Cells Ppplication. *IEEE Trans. Plasma Sci.* **2007**, *35*, 1010−1013.
(50) Yuji, T.; Akatsuka, H.; Mungkung, N.; Park, B. W.; Sung, Y. M. Surface Treatment of TiO_2 Films for Dye-Sensitized Solar Cells Using Atmospheric-Pressure Non-Equilibrium DC Pulse Discharge Plasma Jet. *Vacuum* **2008**, *83*, 124−127.
(51) Zen, S.; Teramoto, Y.; Ono, R.; Oda, T. Development of Low-Temperature Sintering Technique for Dye-Sensitized Solar Cells Combined with Dielectric Barrier Discharge Treatment. *Jpn. J. Appl. Phys.* **2012**, *51*, 6201.
(52) Huang, C.; Chang, Y. C.; Wu, S. Y. Micro-TiO_2 Particles Synthesis by a Novel Atmospheric Pressure Plasma Jet. *J. Chin. Chem. Soc. (Taipei, Taiwan)* **2010**, *57*, 1204−1207.
(53) Huang, C.; Wu, S. Y.; Chang, Y. C.; Pan, C. H.; Tsai, C. Y. The Protection of Flexible DSSC Polymeric Substrate using Atmospheric Pressure Plasma Coating. *J. Chin. Chem. Soc. (Taipei, Taiwan)* **2010**, *57*, 1208−1211.
(54) Hsu, Y.-W.; Li, H.-C.; Yang, Y.-J.; Hsu, C.-W. Deposition of Zinc Oxide Thin Films by an Atmospheric Pressure Plasma Jet. *Thin Solid Films* **2011**, *519*, 3095−3099.
(55) Li, L. L.; Chang, Y. C.; Wu, H. P.; Diau, E. W. G. Characterisation of Electron Transport and Charge Recombination Using Temporally Resolved and Frequency-Domain Techniques for Dye-Sensitised Solar Cells. *Int. Rev. Phys. Chem.* **2012**, *31*, 420−467.
(56) Pearse, R. W. B.; Gaydon, A. G. *The Identification of Molecular Spectra*. 4th ed.; Chapman and Hall: London, 1976; pp 217−220.
(57) Kavan, L.; Yum, J. H.; Grätzel, M. Optically Transparent Cathode for Dye-Sensitized Solar Cells Based on Graphene Nanoplatelets. *ACS Nano* **2011**, *5*, 165−172.
(58) Banks, C. E.; Davies, T. J.; Wildgoose, G. G.; Compton, R. G. Electrocatalysis at Graphite and Carbon Nanotube Modified Electrodes: Edge-Plane Sites and Tube Ends are the Reactive Sites. *Chem. Commun.* **2005**, *7*, 829−841.
(59) Yang, D.; Velamakanni, A.; Bozoklu, G.; Park, S.; Stoller, M.; Piner, R. D.; Stankovich, S.; Jung, I.; Field, D. A.; Ventrice, C. A.; Ruoff, R. S. Chemical Analysis of Graphene Oxide Films after Heat and Chemical Treatments by X-ray Photoelectron and Micro-Raman Spectroscopy. *Carbon* **2009**, *47*, 145−152.
(60) Dreyer, D. R.; Park, S.; Bielawski, C. W.; Ruoff, R. S. The Chemistry of Graphene Oxide. *Chem. Soc. Rev.* **2010**, *39*, 228−240.
(61) Hsu, C. C.; Yang, Y. J. The Increase of the Jet Size of an Atmospheric-Pressure Plasma Jet by Ambient Air Control. *IEEE Trans. Plasma Sci.* **2010**, *38*, 496−499.
(62) Hsu, Y. W.; Yang, Y. J.; Wu, C. Y.; Hsu, C. C. Downstream Characterization of an Atmospheric Pressure Pulsed Arc Jet. *Plasma Chem. Plasma Process.* **2010**, *30*, 363−372.